Dynamics and subseasonal predictability of a blocking event associated with extreme weather over California in February 2023

Benjamin Moore[1], Juliana Dias[1], Stefan Tulich[1,2], Maria Gehne[1,2], Andrew Hoell[1], John Albers[1], Cory Baggett[3], Emerson LaJoie[3]

[1]NOAA Physical Sciences Laboratory
[2]Cooperative Institute for Research in the Environmental Sciences, University of Colorado - Boulder
[3]NOAA Climate Prediction Center

Contact: benjamin.moore@noaa.gov

1. Introduction

- A blocking pattern over the North Pacific (Figs. 1, 2a) resulted in large precipitation accumulations (Fig. 3a), widespread heavy snowfall (Fig. 3b), and prolonged cold conditions (Fig. 3c) over the western U.S. during late February – early March 2023.
- This pattern was poorly represented in subseasonal forecasts.
- Forcing associated with enhanced tropical convection related to a Madden-Julian Oscillation (MJO) event propagating from the Indian Ocean to the western Pacific (Fig. 2b) contributed to the formation of the blocking pattern.
- **Hypothesis:** Errors in the tropics related to the MJO played a major role in the development of errors in subseasonal forecasts of this blocking event.

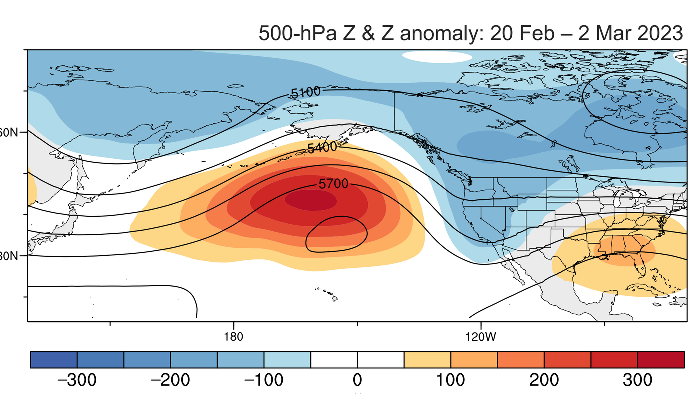

Fig 1: Time-mean 500-hPa Z (m, contours; shading for anomalies) for 20 Feb – 2 Mar 2023 from the ECMWF ERA5 reanalysis.

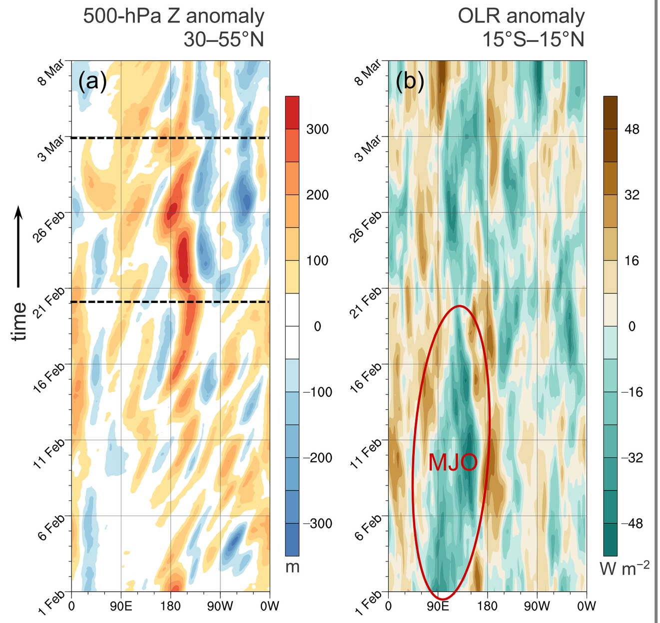

Fig 2: (a) ERA5 500-hPa Z anomaly (m) for 30–55°N; (b) NOAA outgoing longwave radiation (OLR) anomaly ($W\ m^{-2}$) for 15°S–15°N between 1 Feb and 8 Mar 2023.

High-impact weather conditions over the western U.S. during 20 Feb – 2 Mar 2023

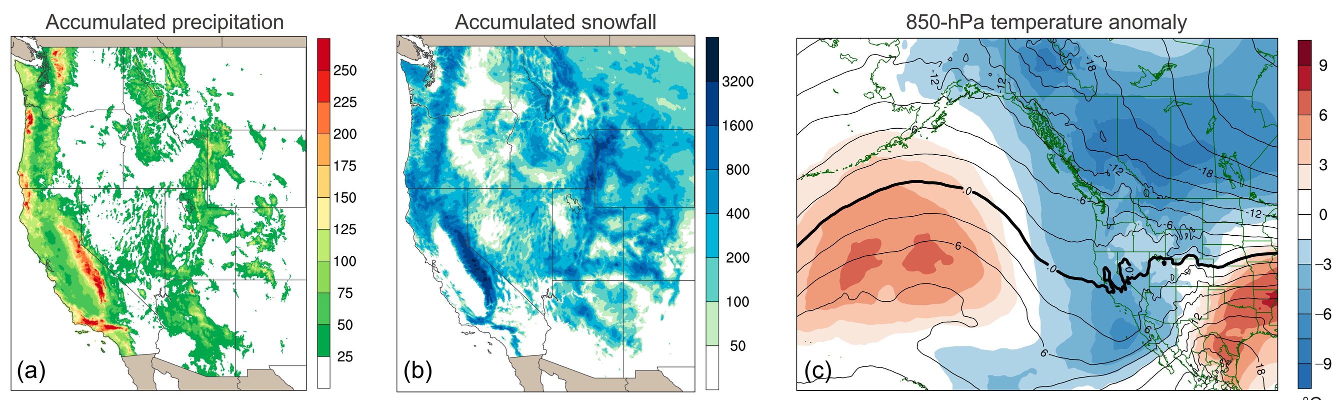

Fig 3: Conditions during 20 Feb – 2 Mar 2023: (a) Accumulated precipitation (mm) from the NOAA Stage-IV analysis, (b) accumulated snowfall (mm) from the NOAA National Gridded Snowfall Analysis, and (c) the time-mean 850-hPa temperature anomaly (°C) from ERA5.

2. Methodology

Model description

- 35-day reforecast experiments conducted with the NOAA Unified Forecast System version HR1 with C96 resolution (~1˚ lat/lon), including the effects of air-sea coupling.
- Three 10-member ensemble forecasts initialized with ERA5 reanalysis at 1200 UTC 1 Feb, 0000 UTC 2 Feb, and 1200 UTC 2 Feb 2023, respectively, yielding a 30-member time-lagged ensemble.

Reforecast experiments

- Wide tropical nudging (**WTR**): Model state variables (i.e., u, v, T, p, q) in the tropics from 10˚S and 10˚N are fully nudged to the ERA5 reanalysis, with the degree of nudging reduced to zero between 10˚S/N and 30˚S/N using a smoothed tapering function (λ).
- Narrow tropical nudging (**NTR**): As in WTR, except that full nudging is restricted to 5˚S–5˚N, and λ is reduced to zero between 5˚S/N and 20˚S/N.
- Control (**CNT**): The model is run freely without nudging.
- ERA5 replay: The model is nudged to ERA5 globally; this run serves as the verification dataset.

3. Impacts of tropical nudging on subseasonal forecast errors

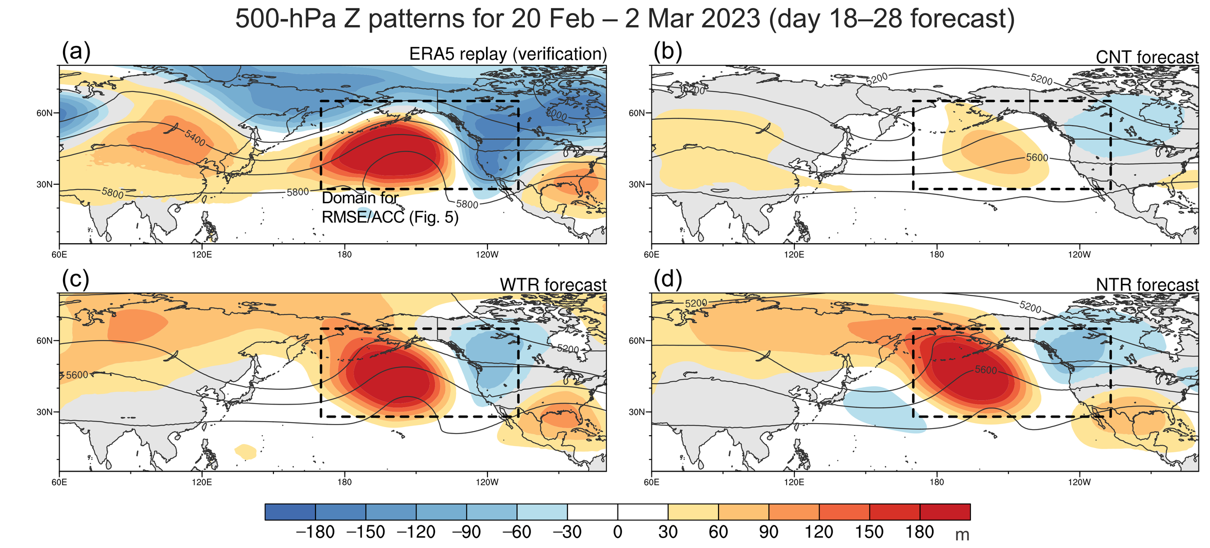

Fig. 4: Time-mean 500-hPa Z (m, contours; shading for anomalies) for 20 Feb – 2 Mar 2023 (day 18–28 forecast) from: (a) the ERA5 replay (i.e., the verification), (b) the CNT ensemble mean, (c) the WTR ensemble mean, and (d) the NTR ensemble mean. The dashed box indicates the domain for the metrics in Fig. 5. Anomalies hereinafter are computed relative to a lead-dependent UFS reforecast climatology for 1994–2022.

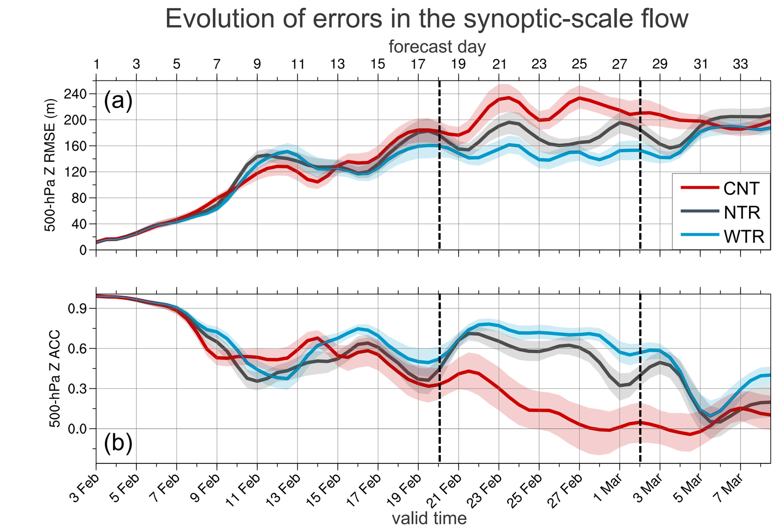

Fig. 5: (a) The root-mean-square error and (b) anomaly correlation coefficient for the forecast 500-hPa Z (domain in Fig. 4) averaged over the ensemble members (95% confidence interval shaded).

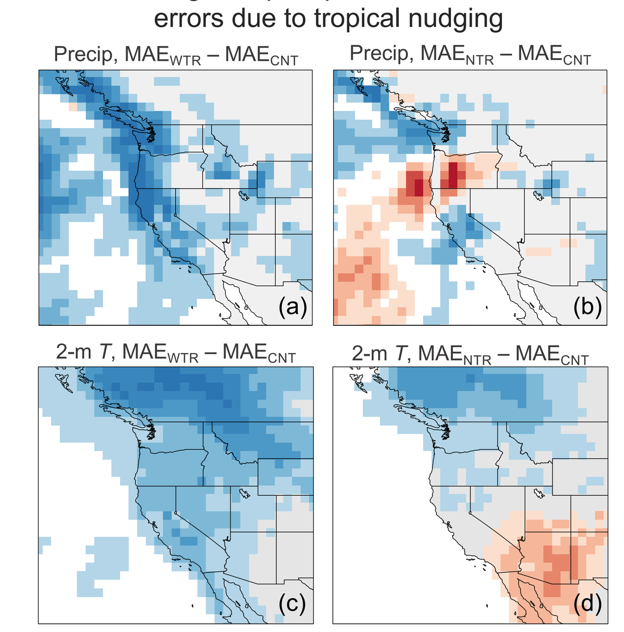

Fig. 6: Difference in the mean absolute error of (a),(b) accumulated precipitation and (c),(d) 2-m temperature (°C) between the nudged and CNT forecasts for 20 Feb – 2 Mar 2023 (day 18–28 forecast).

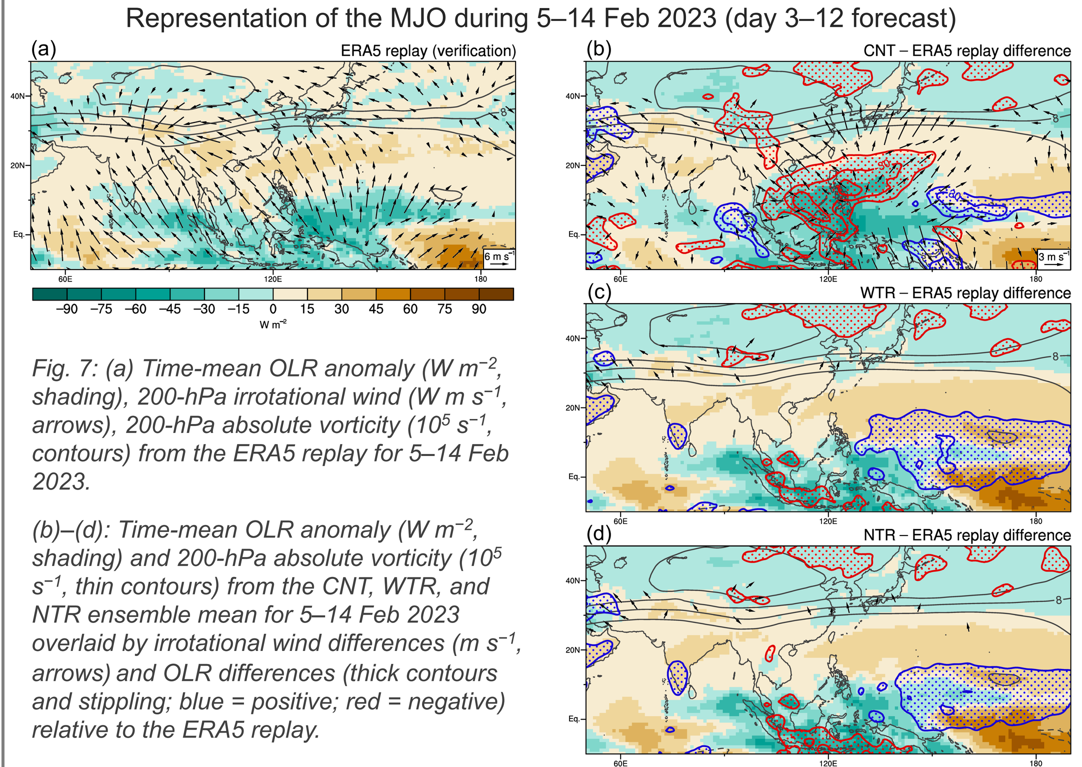

Fig. 7: (a) Time-mean OLR anomaly ($W\ m^{-2}$, shading), 200-hPa irrotational wind ($W\ m\ s^{-1}$, arrows), 200-hPa absolute vorticity ($10^5\ s^{-1}$, contours) from the ERA5 replay for 5–14 Feb 2023.

(b)–(d): Time-mean OLR anomaly ($W\ m^{-2}$, shading) and 200-hPa absolute vorticity ($10^5\ s^{-1}$, thin contours) from the CNT, WTR, and NTR ensemble mean for 5–14 Feb 2023 overlaid by irrotational wind differences ($m\ s^{-1}$, arrows) and OLR differences (thick contours and stippling; blue = positive; red = negative) relative to the ERA5 replay.

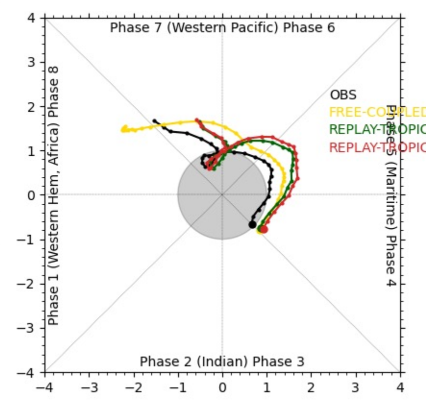

Fig. 8: The Real-time OLR MJO Index (ROMI) phase space diagram for 2 Feb – 7 Mar 2023 (day 1–33 forecast) for the ERA5 replay (black), and the CNT (yellow), WTR (green), and NTR (red) ensemble means.

Key points

- Both WTR and NTR produce significant reductions in 500-hPa Z errors and improved representation of the blocking pattern relative to CNT (Figs. 4, 5).
- Improved forecasts of the synoptic-scale flow result in reductions in precipitation and 2-m temperature errors (Fig. 6).
- WTR exhibits greater error reductions than NTR.
- The MJO evolution is represented well in CNT, WTR, and NTR (Fig. 8), but CNT exhibits large errors in the structure, intensity, and location of the convection and divergent outflow (Fig. 7).

4. Synoptic-dynamic diagnosis of the impacts of tropical nudging

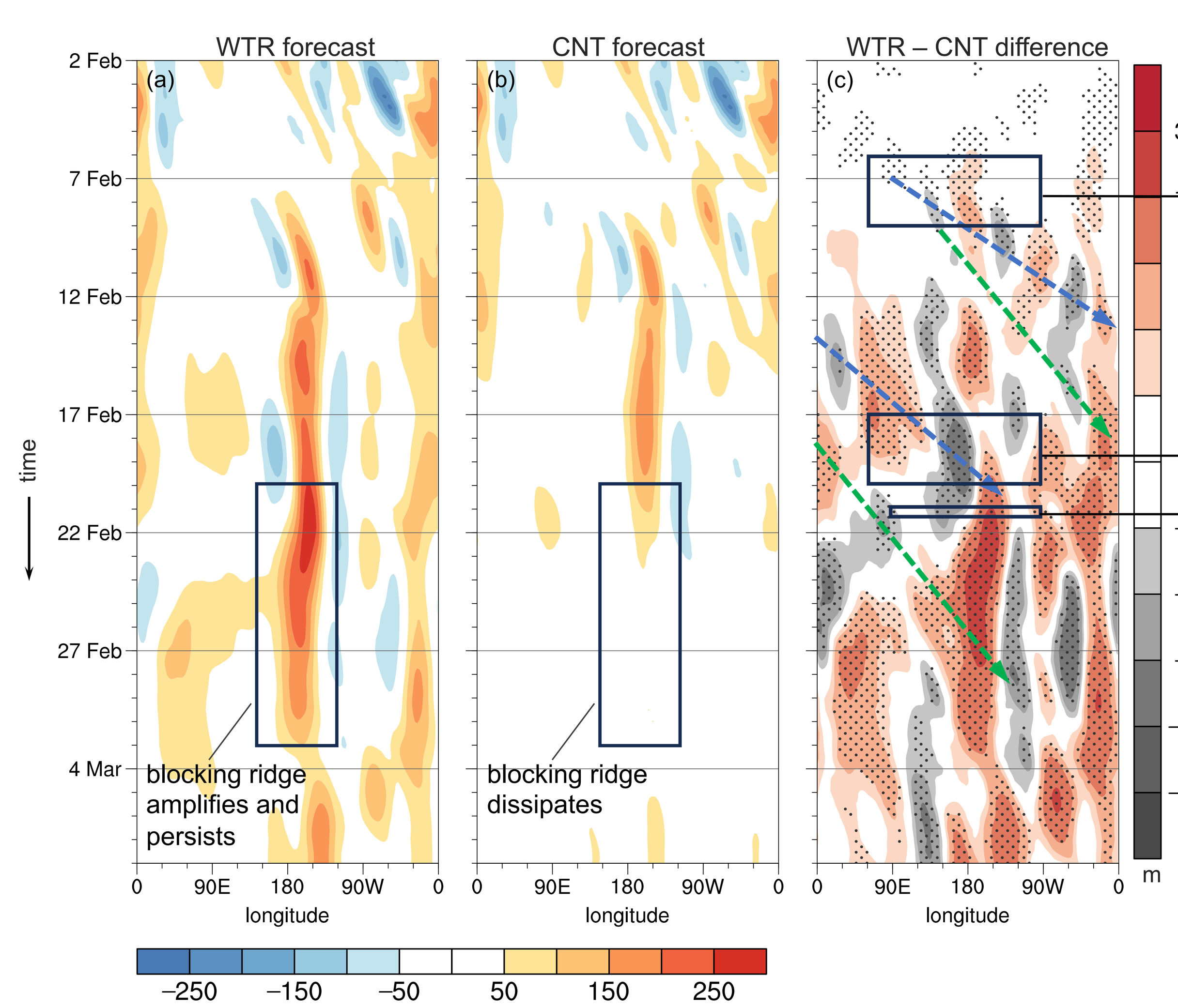

Fig. 9: Ensemble-mean 500-hPa Z anomalies averaged in the 30–60°N band for (a) the WTR forecast and (b) the CNT forecast. (c) Ensemble-mean difference in 500-hPa Z between the WTR and CNT forecasts; stippling denotes differences that are statistically significant ($p < 0.05$) based on a bootstrap resampling test.

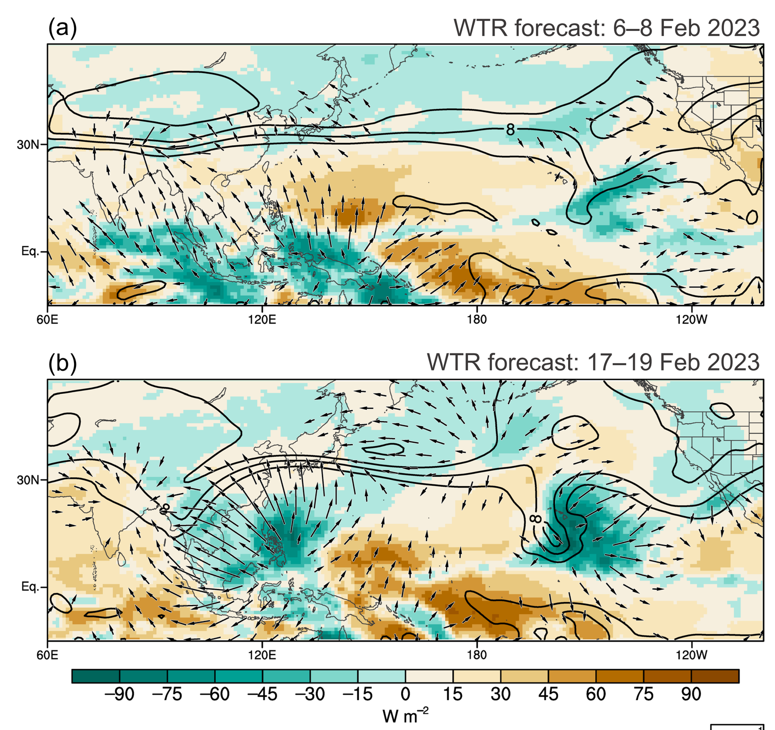

Fig 10: Ensemble-mean OLR anomaly ($W\ m^{-2}$, shading), 200-hPa absolute vorticity ($10^5\ s^{-1}$, contours), and 200-hPa irrotational wind ($m\ s^{-1}$, arrows) from the WTR forecast averaged for (a) 6–8 Feb and (b) 17–19 Feb 2023.

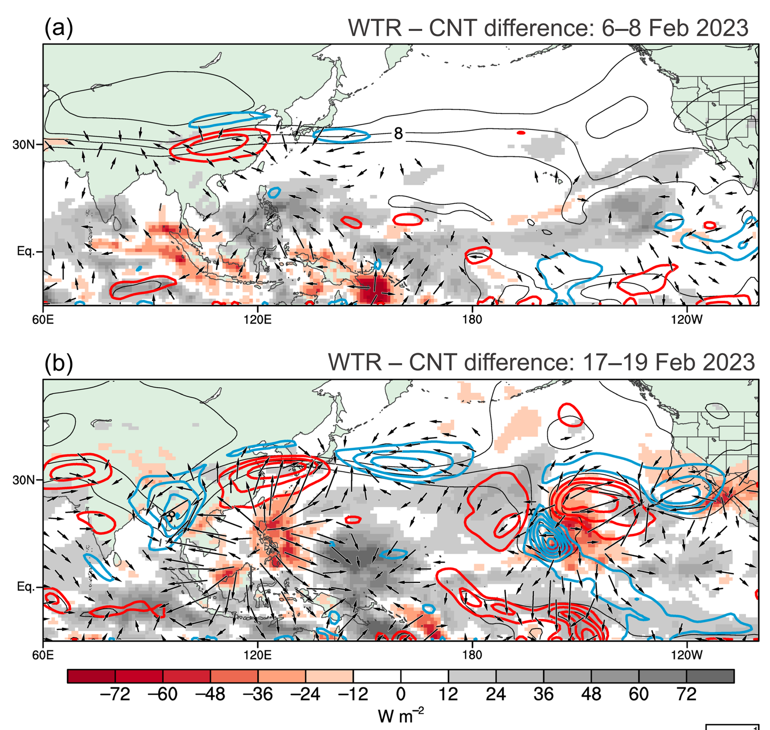

Fig 11: Ensemble-mean differences between the WTR and CNT forecasts averaged for (a) 6–8 Feb and (b) 17–19 Feb 2023: OLR ($W\ m^{-2}$, shading), 200-hPa absolute vorticity ($10^5\ s^{-1}$, contours; blue = positive; red = negative), and 200-hPa irrotational wind ($m\ s^{-1}$, arrows).

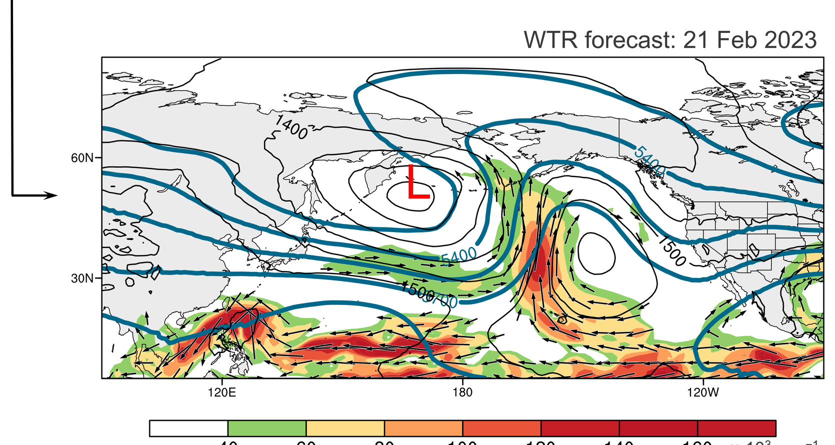

Fig 12: Ensemble-mean 850-hPa water vapor flux ($10^3\ m\ s^{-1}$; shading and arrows), 850-hPa Z (m, thin contours), and 500-hPa Z (m, thick contours) from the WTR forecast valid on 21 Feb 2023.

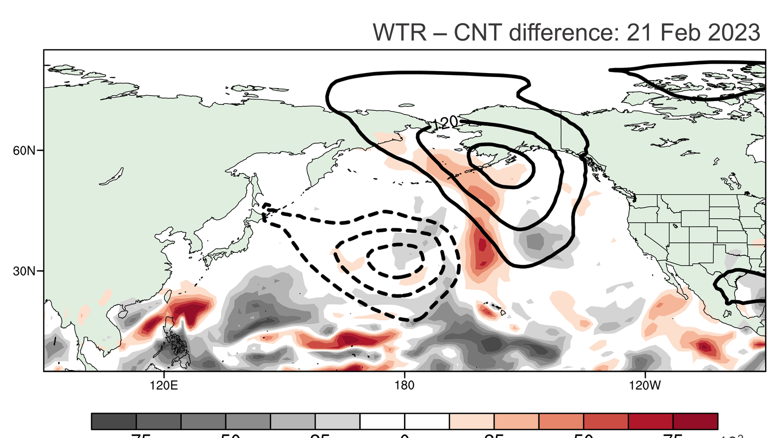

Fig 13: Ensemble-mean differences between the WTR and CNT forecasts valid on 21 Feb 2023: 850-hPa water vapor flux ($10^3\ m\ s^{-1}$; shading) and 500-hPa Z (m, contours; dashed for negative values).

Key points

- WTR captures the amplification and persistence of the blocking pattern after 20 Feb; CNT does not (Fig. 9).
- Extratropical circulation differences between WTR and CNT emerge in weeks 1–2 of the forecast in association with differences in the location and structure of MJO-related convection (Figs. 10a, 11a).
- Circulation differences subsequently propagate downstream around the Northern Hemisphere as Rossby wave packets (blue & green arrows in Fig. 9c).
- Differences grow rapidly between 18 and 22 Feb in response to a stronger (weaker) interaction between a trough and MJO-related convection in WTR (NTR) (Figs. 10b, 11b).
- WTR exhibits more intense downstream baroclinic development over the central North Pacific during 20–22 Feb, resulting in stronger amplification of the blocking ridge (Figs. 12, 13).

5. Conclusions

- Nudging the tropics to reanalysis results in significant error reductions in the subseasonal (i.e., week 3–4) forecast of the late Feb – early Mar 2023 blocking event and its impacts over the western U.S.
- Extratropical circulation differences between the nudged and control forecasts emerge in weeks 1–2 in association with differences in the structure, intensity, and location of MJO-related convection and divergent outflow; these circulation differences propagate and evolve in the form of Rossby wave packets.
- The nudged and control forecasts diverge from each other in association with differences in baroclinic development over the central North Pacific, with the control forecast exhibiting much weaker development and thereby failing to capture the amplification and persistence of the blocking ridge.
- The differences in baroclinic development and blocking occur in response to upstream differences in the interaction between a trough and MJO-related convection over the western Pacific.